Progress in Nuclear Energy 83 (2015) 336–346

Contents lists available at ScienceDirect

Progress in Nuclear Energy

journal homepage: www.elsevier.com/locate/pnucene

Numerical simulation of single bubble condensation in subcooled flow using OpenFOAM

Qingyun Zeng [a], Jiejin Cai [a, *], Huaqiang Yin [b], Xingtuan Yang [b], Tadashi Watanabe [c]

[a] Sino-French Institute of Nuclear Engineering & Technology, Sun Yat-sen University, Guangzhou 510275, China
[b] Institute of Nuclear and New Energy Technology of Tsinghua University, Key Laboratory of Advanced Reactor Engineering and Safety, Ministry of Education, Beijing 100084, China
[c] Research Institute of Nuclear Engineering, University of Fukui, Kanawa-cho 1-2-4, Tsuruga-shi, Fukui 914-0055, Japan

ARTICLE INFO

Article history:
Received 14 February 2015
Received in revised form
31 March 2015
Accepted 20 April 2015
Available online

Keywords:
Bubble behavior
Condensation
OpenFOAM
CLSVOF method

ABSTRACT

The single condensing bubble behavior in subcooled flow has been numerical investigated using the open source code OpenFOAM. A coupled Level Set (LS) and Volume of Fluid (VOF) method (CLSVOF) model with a phase change model for condensation was developed and implemented in the code. The simulated results were firstly compared with the experimental results, they were in great agreements, and thus the simulation model was validated. The validated numerical model was then used to analyze the condensing bubble deformation, bubble lifetime, bubble size history, condensate Nusselt number and other interesting parameters with different variables in subcooled flow. The numerical results indicated that the initial bubble size, subcooling of liquid and system pressure play an important role to influence the condensing bubble behaviors significantly and bubble will be pierced when the subcooling and initial diameter reach a certain value at the later condensing stage. The bubble diameter history and condensate Nusselt number were found in good agreement with the empirical correlation. The drag force coefficient was predicted well by introducing a reduced drag coefficient.

1. Introduction

In the nuclear reactors, the in-vessel bubble dynamics would be very important for the reactor safety and control analysis because it would influence the void reactivity feedback characteristics for the reason of the coupling thermal–hydraulics and neutronics. The steam bubble condensation has thus attracted many researchers' attention in the nuclear engineering field.

The research is focused on the theoretical analysis, experimental analysis and numerical simulation. Robin and Snyder (1970) made a theoretical analysis of bubble dynamics for an artificially produced vapor bubble in a turbulent stream, gave a mathematical model for the artificially produced vapor bubble growing on a surface and into a turbulent subcooled stream flowing parallel to the surface. Kalman (2003) developed a theoretical model for bubble condensation in immiscible and miscible liquids. There have been many experimental analyses on the condensing bubble behavior (Lin and Chen, 2012). Ju et al. (2000) used the holographic interferometer and high speed camera to measure the heat transfer coefficients around steam bubbles and tried to understand the heat transfer mechanism for the direct contact condensation in Core Makeup Tanks. Harada et al. (2010) carried out the visualization experiments to investigate the dynamics of vapor bubbles generated in water pool boiling. Morita et al. (2008) did a series of transient bubble behavior experiments dedicated to condensation phenomena with non-condensable gases to verify the fast reactor safety analysis code SIMMER-III for transient bubble behavior with condensation.

In the experimental studies, bubble behavior with bubble size history, shape, velocity, collapse time and interfacial heat transfer coefficient was investigated under various conditions. However, it is impossible to obtain complete information about the bubble behavior because the shape and the area of the interface are very complicated and difficult to measure. Moreover, bubble condensation significantly affects the change of interface, which complicates the bubble behavior even more. Therefore, it is necessary to

* Corresponding author. Sino-French Institute of Nuclear Engineering & Technology, Sun Yat-sen University, Tangjiawan, Xiangzhou, Zhuhai 519082, China.
E-mail address: chiven77@hotmail.com (J. Cai).

http://dx.doi.org/10.1016/j.pnucene.2015.04.011
0149-1970/

Nomenclature

C_γ	adjustable compression coefficient
Cd	drag coefficient
Cdr	reduced drag coefficient
D_0	initial diameter of bubble, mm
D_b	equivalent diameter of bubble, mm
Fo	Fourier number, –
H	Heaviside function
Ja	Jakob number, –
Pr_l	Prandtl number, –
M	number of grid points
Nu_c	condensate Nusselt number, –
Re	bubble Reynolds number, –
R_{gas}	gas constant, J/(kg K)
R_{int}	interfacial heat resistance, (K m^2)/W
T	temperature, K
U	velocity, m/s
U_r	the artificial compression velocity
h_{lv}	specific heat of vaporization, J/kg
$\dot{h}$	enthalpy source term, W/m^3
Δx	mesh step size, –
Υ	artificial finite thickness
Γ	small dimensionless number; $\Gamma = 0.75\Delta x$
α	volume fraction of one phase, –
β	bubble diameter history
δ	Dirac function
ε	interface thickness
λ	thermal conductivity, W/(m K)
μ	dynamic viscosity, Pa s
ρ	density, kg/m^3
$\dot{\rho}$	source term, kg/m^3 s
σ	surface tension, N/m
τ	artificial time
$\Delta\tau$	artificial time step
ϕ	Level Set field, –
χ	condensation coefficient, –

Subscripts

b	Bubble
l	liquid phase
v	vapor phase
int	Interface
sat	Saturation

carry out numerical simulations for condensing bubble behavior as a complement to experiments. Tian et al. (2010) simulated single steam bubble condensation behaviors in subcooled water by using the Moving Particle Semi-implicit (MPS) method and MPS is further used to simulate the bubble dynamics during flow boiling (Chen et al., 2010), coalescence of bubble pairs rising in a stagnant liquid (Chen et al., 2011), single bubble rising behavior in liquid metal (Zuo et al., 2013), etc. Pan et al. (2012) numerically investigated the behavior of condensing single vapor bubble in subcooled boiling flow within two different vertical rectangular channels using the Volume of Fluid (VOF) multiphase flow model. Patel et al. (2014) tried to numerical model the low-Reynolds number direct contact condensation in a suppression pool test facility by using the Eulerian two-fluid approach of interpenetrating continua without interfacial tracking.

Recently, an open source CFD package, OpenFOAM (2014) attracts more and more researchers' interests for the reason of being free and convenient. The OpenFOAM library allows implementation of fields, equations and operator discretization using a high-level C++ coding interface. Descriptions of the available mathematical operators, discretization implementations, matrix solvers and the general use of the software can be found. It has been successfully applied in the nuclear engineering fields (Nath and Verma, 2014; Patel et al., 2014; Jareteg et al., 2014; Aufiero et al., 2014). We also used OpenFOAM to simulate the temperature stratification phenomena in ROSA-V/LSTF, which is a PWR simulator with a volume scaling ratio of 1/48, at the Japan Atomic Energy Agency (JAEA) (Cai et al., 2010; Cai and Watanabe, 2011), simulate the rising characteristics of bubbles(Cai et al., 2013), simulate the motions of free interface and its coupling with bubble in oscillating two-phase flow field (Zeng et al., 2013), simulate the bubble behavior under nonlinear oscillation (Zeng and Cai, 2014). In this paper, we summarizes the new results of our studies on using OpenFOAM to simulate the bubble condensation in subcooled boiling flow.

The remainder of this paper is organized as follows. Section 2 describes the Computational method and models; Section 3 gives some results and discussions and the conclusions are summarized in Section 4.

2. Computational method and models

2.1. Governing equations

In this study, the two phase flow is treated as incompressible and immiscible Newtonian fluid. Governing equations for the two phase flow field are the equation of continuity, the incompressible Navier–Stokes equation and the equation of energy balance for:

$$\nabla\cdot(\rho\mathbf{u}) = \dot{\rho} \tag{1}$$

$$\rho\frac{d\mathbf{u}}{dt} + \nabla\cdot(\mathbf{u}\cdot\rho\mathbf{u}) = -\nabla p + \nabla\cdot\boldsymbol{\tau} + f_{\mathbf{g}} + f_{\sigma} \tag{2}$$

$$\frac{d\rho c_p T}{dt} + \nabla\cdot\left(\mathbf{u}\cdot\rho c_p T\right) = \nabla\cdot(\lambda\nabla T) + \dot{h} \tag{3}$$

The source term on the right side of Eq. (1) represents the local density rate caused by phase change. It is mentioned that, the mass is still globally conserved in spite of the local source terms (all of the mass removed on the vapor side of the interface reappears on the liquid side). In Eq. (2), τ is the viscous stress tensor, for incompressible Newtonian fluid $\boldsymbol{\tau} = \mu(\nabla\mathbf{U} + \nabla\mathbf{U}^T)$; the momentum source terms f_g and f_σ, are gravity and the surface tension force, respectively. The surface tension force is modeled according to the so-called Continuous-Surface-Force (CSF) method (Brackbill et al., 1992). Source term on the right side of Eq. (3) expresses the heat that is produced by condensation or removed by evaporation.

In our previous researches, the simulation was based on VOF model (Cai et al., 2010; Cai et al., 2013; Cai and Watanabe, 2011; Zeng et al., 2013; Zeng and Cai, 2013) within OpenFoam. Sussman and Puckett (2000) presented a Coupled Level Set and Volume of Fluid (CLSVOF) method and got better results than VOF method. The aim of this method is to benefit from the mass conservation of VOF, the smoothed curvature and the Dirac function available in the surface tension model of Level Set (LS). CLSVOF is also successfully used to simulate the bubble growth and detachment (Albadawi et al., 2013). This paper thus tried to implement CLSVOF with a

phase change model (Hardt and Wondra, 2008) in OpenFOAM and then did the simulations.

In contrast to VOF, the LS method provides a sharp interface and a smooth transition in the physical properties across the interface and also confines the effect of the volumetric surface force to a narrow region around the interface by using the Dirac function.

Although the two separate fields, VOF and LS, are defined to represent the fluid domain, only the VOF advection equation is solved meanwhile the LS function is used to adapt the surface tension force model and physical properties. The coupling includes several steps (Albadawi et al., 2013) as follow.

Like the VOF method, the function α is defined as volume fraction of one phase shown in Eq. (4), which is calculated by solving the transport equation Eq. (5).

$$\alpha(x,t)=\begin{cases}1, & \text{liquid}\\ 0, & \text{vapor}\\ 0<\alpha<1, & \text{interface}\end{cases} \tag{4}$$

$$\frac{\partial\alpha}{\partial t}+\nabla\cdot(\mathbf{u}\alpha)=\frac{\dot{\rho}}{\rho}\alpha \tag{5}$$

The first step of the coupling is to assign an initial value to the Level Set function using the advected VOF fraction function and assuming that the interface position is defined at the contour $\alpha = 0.5$.

$$\phi_0=(2\alpha-1)\Gamma \tag{6}$$

where Γ is a small dimensionless number whose value depends on the mesh step size Δx: $\Gamma = 0.75\Delta x$. With this treatment a signed function is generated since it has a positive value in the liquid and a negative value in the gas.

The second step is re-distanced ϕ_0 by solving the following re-initialization equation:

$$\begin{cases}\dfrac{\partial\phi}{\partial\tau}=S(\phi_0)(1-|\nabla\phi|)\\ \phi(x,\ 0)=\phi_0(x)\end{cases} \tag{7}$$

The steady state solution of the Eq. (3) satisfies the sign distance function condition $|\nabla\phi| = 1$. The artificial time step $\Delta\tau$ is chosen as $0.1\Delta x$. The stop criterion for the iteration of re-initialization step is to satisfy Eq. (8):

$$E=\frac{\sum_{|\phi^N|<\Upsilon}(\phi^{N+1}-\phi^N)}{M}<\Delta\tau\Delta x^2 \tag{8}$$

where Υ is an artificial finite thickness adjacent to the interface, e.g. $\Upsilon = 5\Delta x$. M is the number of grid points that satisfies $|\phi^N|<\Upsilon$.

By developing such a continuous function, more accurate surface tension model and physical properties can be achieved.

$$f_\sigma=\sigma\delta(\phi)\kappa\nabla\phi \tag{9}$$

$$\gamma=\gamma_l H+\gamma_v(1-H) \tag{10}$$

where γ represents a variable for any of the material properties, and δ is a Dirac-like function used to limit the influence of the surface tension to a narrow region around the interface and H is the Heaviside function, defined as:

$$\delta(\phi)=\begin{cases}0, \text{if}|\phi|>\varepsilon\\ \dfrac{1}{2}(1+\cos(\pi\phi/\varepsilon))\Big/\varepsilon, \text{if}|\phi|\le\varepsilon\end{cases} \tag{11}$$

$$H=\begin{cases}0, \text{if}\,\phi<-\varepsilon\\ \dfrac{1}{2\varepsilon}\left[1+\dfrac{\phi}{\varepsilon}+\dfrac{1}{\pi}\sin\left(\dfrac{\pi\phi}{\varepsilon}\right)\right], \text{if}|\phi|\le\varepsilon\\ 1, \text{if}\,\phi>\varepsilon\end{cases} \tag{12}$$

2.2. Phase change model

The phase change model is modeled based on the work of Hardt and Wondra (2008). Mass flux at the liquid–vapor interface is calculated as:

$$j=\frac{T_i-T_{sat}}{R_{int}h_{lv}} \tag{13}$$

where T_i is the temperature of the phase boundary, T_{sat} the saturation temperature, h_{lv} the enthalpy difference of two phases, and R_{int} is the heat resistance of the liquid–vapor interface. Based on the considerations of Schrage (1953), R_{int} can be expressed by:

$$R_{int}=\frac{2-\chi}{\chi}\frac{\sqrt{2\pi R_{gas}}}{h_{lv}}\frac{T_{sat}^{3/2}}{\rho_v} \tag{14}$$

More details on the phase change model can be referenced to Hardt and Wondra (2008), Kunkelmann and Stephan (2009).

The models are implemented into the OpenFOAM standard solver interFoam, a good evaluation on this two-phase flow solver can be referenced to Deshpande et al. (2012). The VOF method in the solver does not solve Eq. (5) implicitly and reconstruct the two-phase interface, but using a multidimensional universal limiter with explicit solution (MULES) algorithm (OpenFOAM, 2014), together with an artificial interface compression (AIC) algorithm, ensures a sharp interface and limits the volume fraction field to values between 0 and 1. The artificial interface compression term $\nabla\cdot(\alpha(1-\alpha)\mathbf{U}_r)$ is introduced into Eq. (5):

$$\frac{\partial\alpha}{\partial t}+\nabla\cdot(\mathbf{u}\alpha)+\nabla\cdot(\alpha(1-\alpha)\mathbf{U}_r)=\frac{\dot{\rho}}{\rho}\alpha \tag{15}$$

U_r is the artificial compression velocity, given by:

$$\mathbf{U}_r=\mathbf{n}_f\min\left[C_\gamma\frac{|\phi|}{|S_f|},\max\left(\frac{|\phi|}{|S_f|}\right)\right] \tag{16}$$

where n_f is the normal vector of the cell surface, ϕ is the mass flux, S_f is the cell surface area and C_γ is an adjustable compression coefficient which we set to 1. The term α (1-α) ensures that this artifact is only active in the thin interfacial region. Evidence on the accuracy of the MULES and AIC can be found in Rusche (2002) and Deshpande et al. (2012).

3. Results and discussion

In this study, the three-dimensional space domain is set as $2D_0 \times 4D_0 \times 2D_0$, corresponding to the x, y, z directions (the y direction is chosen as the upward flow direction), shown in Fig. 1, herein D_0 is the initial diameter of the bubble, and the sphere bubble is initialized in the position (D_0, D_0, D_0) at the beginning.

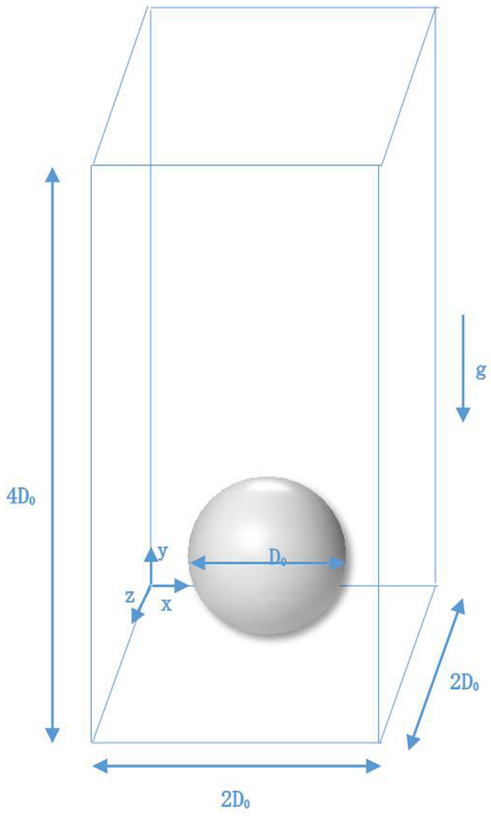

Fig. 1. The three-dimensional simulation domain.

3.1. Mesh resolution dependence

A mesh resolution analysis is performed to test the mesh dependence for bubble condensation in subcooled flow. Sizes of the meshes used in these analyses are M1 (50 × 100 × 50), M2 (64 × 128 × 64), M3 (80 × 160 × 80), M4 (100 × 200 × 100) respectively represent 25, 32, 40 and 50 cells across the initial diameter. Fluid properties such as densities, viscosities and surface tension are properties of saturated steam and subcooled water with a subcooled degree of 10 K. Fig. 2 shows the slices of bubble in the middle of z direction during the condensing process, it is noted that

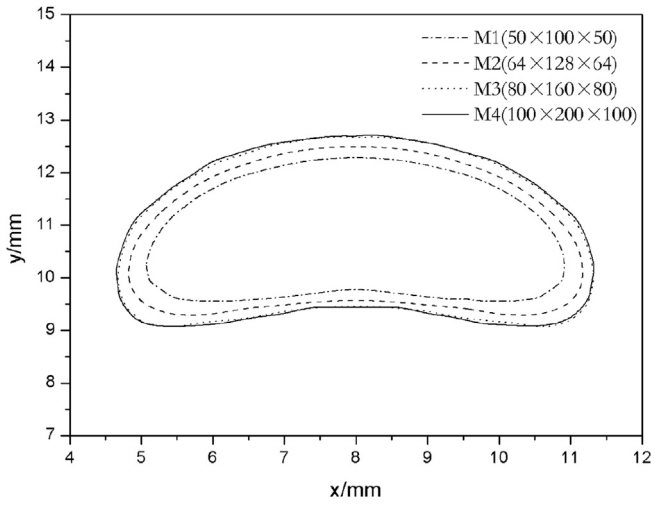

Fig. 2. Grid dependence test at various grids on condensing bubble.

the condensing bubble has a large deformation at the chosen moment and condition. It can be seen obvious that bubble shape becomes stable with mesh M3 and M4. The fluctuation of M3 and M4 is so smaller compared to the mean value, and hence it is negligible. So the bubble is resolved using mesh M3 in this study.

3.2. Comparison with the experimental results

In many well recognized previous experiments, the shape and size history of bubble were recorded qualitatively and quantificationally (Kamei and Hirata, 1990; Kalman and Mori, 2002). In the experiment of Pan et al. (Pan et al., 2012), the shape and size history of bubble condensation with different bubble initial diameter (D_0), subcooled degree and system pressure were well recorded. In order to validate our numerical models, cases are carried out and compared with their published experimental results under the corresponding condition as shown in Table 1. The comparison of bubble diameter history is shown as Fig. 3, and the bubble shape of Case 3 is contrasted in Fig. 4. It can be seen that the numerical result is in reasonable agreement with the experimental result. Thus this numerical simulation for bubble condensation is performed well and the simulation model is validated.

3.3. Bubble shape in condensation

Bubble shape is a key factor to study the two phase flow characteristic, the stable bubble shape was determined by three dimensionless Morton number, Eotvos number and Reynolds number (Clift et al., 1978). However, heat and mass transfer will be happened during bubble condensation, which brings a heterogeneous void fraction disappearance and results in a very different unstable bubble shape.

Fig. 5 shows 3-D bubble deformation process obtained through the CLSVOF model from OpenFOAM in this study and the comparison with Kamei's typical experimental records (Kamei and Hirata, 1990). The bubble initial diameter is 8 mm and subcooled degree is of 10 K under the system pressure of 2×10^5 Pa. From the condensation process in Fig. 5, it can be seen that the bubble goes through a process of hemispherical, ellipsoidal and spherical shapes under this specific condition. Bubble becomes to flatten at the beginning due to the action of buoyancy, and then a hemispherical shape appears because of the influence of mass transfer. Later the top of the bubble begins to flatten, an ellipsoidal shape is attained. At the final stage, the bubble returns to a spherical shape because of increasing influence of interfacial surface tension. The bubble shape history is generally consistent with the experimental results.

With the increase of subcooled degree, interfacial heat and mass transfer of bubble will be greatly enhanced, corresponding bubble lifetime is dramatically reduced as well. A comparison of bubble shape sequences under different subcooled degree but same other condition can be seen in Fig. 6. It is indicated that bubble lifetime is much shorter under high subcooled degree, and the bubble rise distance is greatly reduced because of much shorter lifetime. As interfacial heat and mass transfer strengthens, the condensation induced interfacial motion rather than buoyancy plays the dominant role in bubble deformation under higher subcooled degree conditions. And this is why bubble maintain spherical or ellipsoidal with less deformation at high subcooled degrees.

Fig. 7 shows bubble shape deformed processes of two different initial size of bubble under same subcooled condition. For small bubble, bubble goes through spherical, hemispherical, and ellipsoidal shapes successively and final back to spherical shape and then disappears. While for large bubble, bubble becomes

Table 1
Operation conditions of experiment and simulation.

Case	System pressure (Mpa)	Subcooled degree (K)	Mass flux (kg/m^{2}s)	Bubble initial diameter (mm)
1	0.106	8.7	100.0	1.024
2	0.101	12.8	118.0	0.950
3	0.130	25.0	400.0	1.008

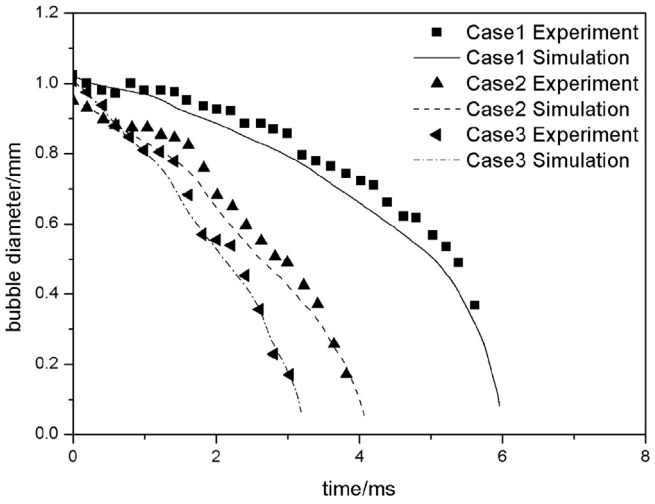

Fig. 3. Bubble diameter history comparison between experiment (Kamei and Hirata, 1990) and simulation.

hemispherical at first and later ellipsoidal and then hollow and pierced finally.

Based on the analyses above, mainly three condensing processes are classified. Fig. 8 shows shape and flow field around bubbles with 1 mm, 6 mm and 20 mm initial diameter of those two processes. It is noted that the figures shown are slices of bubble in the middle of z direction. Fig. 8(a) shows a condensing process bubble remains spherical while Fig. 8(b) shows a condensing process bubble goes through spherical, hemispherical, ellipsoidal and spherical shapes successively and Fig. 8(c) shows a condensing process bubble goes through hemispherical, ellipsoidal shape but becomes pierced finally.

Bubble shape is determined by drag force, buoyancy, surface tension and inertial force induced by the liquid around the bubble due to condensation. Among those forces, surface tension acts as the force to maintain spherical shape while others make bubble deformed. The inertial force induced by condensation is closely related to the subcooled degree of liquid thus higher subcooled degree will induce a greater inertial shock. According to Young–Laplace equation, the internal pressure of smaller bubble induced by the surface tension will be higher than the inertial force while that of larger bubble will be lower. Thus small bubble maintains a spherical shape as shown in Fig. 8(a). Bubble deforms at first in Fig. 8(b) because internal pressure is lower than inertial force, then internal pressure becomes larger as bubble condenses, bubble becomes spherical shape again. Bubble deforms harder and become dimpled at first in Fig. 8(c) because of the larger initial diameter. Then as the top of the bubble begins to flatten and sagged bottom begins to condense, bubble becomes thinner in the middle thus pierced finally.

3.4. Bubble diameter history and lifetime

Bubble diameter history $\beta = D_b/D_0$ in condensation under varies conditions are shown in Fig. 9, where D_b is the instantaneous bubble equivalent diameter and D_0 is the initial bubble diameter. The equivalent diameter is defined as the diameter of a sphere with the same volume as the bubble. The solid lines show bubble diameter history of different initial size with subcooled degree of 10 K, while dash lines of 20 K and dot lines of 50 K. The square symbols present β of different subcooled degree with initial size of 2 mm, while diamond symbols of 10 mm and up-triangle symbols of 20 mm. It is found that for bubbles with same initial size, β decreases faster as subcooled degree increases, which leads to reduction of the bubble lifetime. For those bubbles with different initial size but same subcooled condition, the larger bubble is with slower β decrement and thus longer lifetime. It is mainly because larger bubble is with bigger quality, and it will survive longer time at the same condition during the condensation process. A phenomenon should be noted that, for large initial size bubble, a rapid decrease will occur at the end of β curve (e.g. up-triangle solid line, up-triangle dash line, diamond dash line). One explanation is that bubble will be pierced under high subcooled degree and large initial diameter and its interface will be much larger under this condition, thus the heat transfer will intensify and the equivalent diameter will decrease rapidly.

The comparison of condensing bubble lifetime with experimental results (Kamei and Hirata, 1986) under different system pressure, subcooled degrees and initial bubble size is shown in

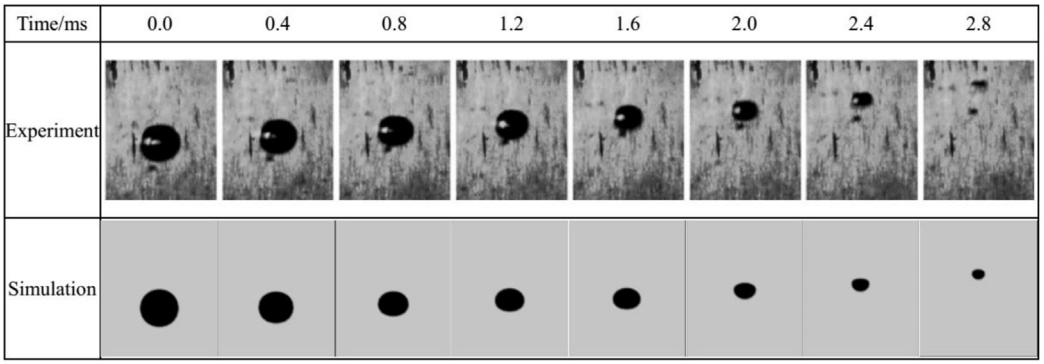

Fig. 4. Bubble shape history comparison between experiment (Kamei and Hirata, 1990) and simulation in case 3.

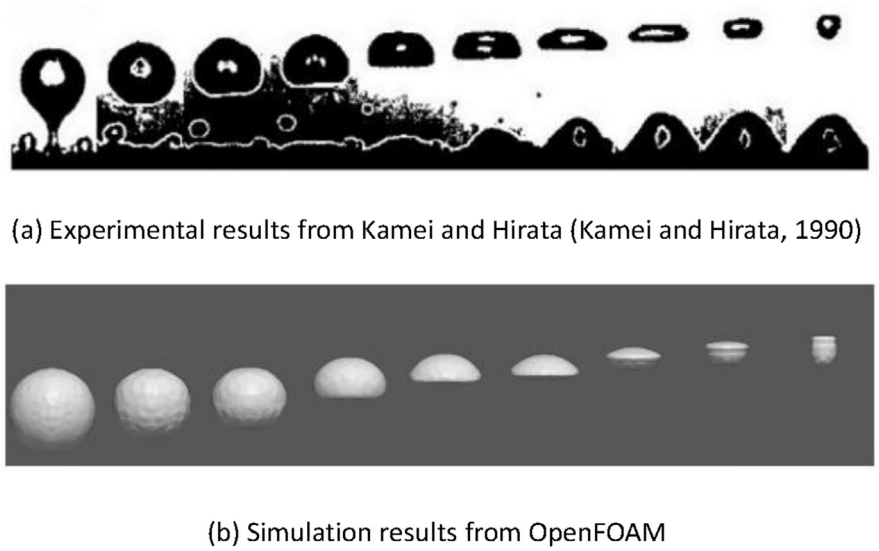

Fig. 5. Bubble shape history comparison during condensation (D_0 = 8 mm, ΔT_{sub} = 10 K).

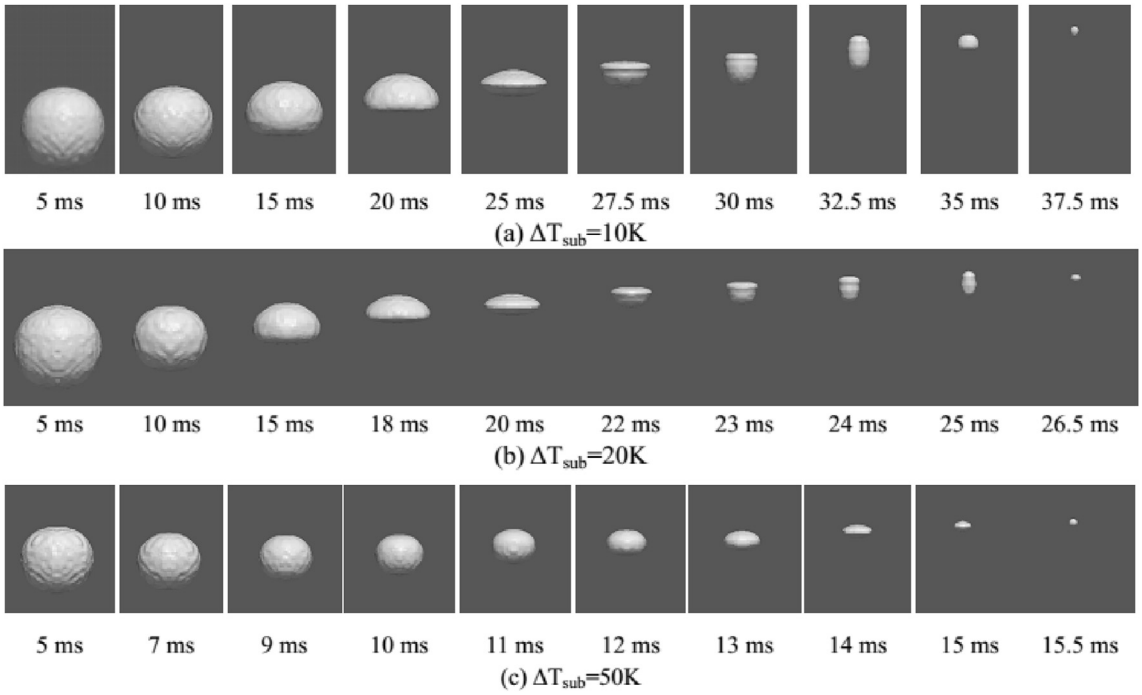

Fig. 6. Bubble shape sequences with 6 mm in initial diameter during condensation (P = 1.55 MPa).

Fig. 10. The computational results match the experimental results greatly. It can be found from both computational and experimental results that condensing bubble lifetime is nearly proportional to the initial bubble size. As mentioned in Section 3.3, bubble lifetime decreases with increasing subcooled degree in both low and high system pressure because of the enhanced interfacial heat and mass transfer. Besides, a higher system pressure provides a longer bubble lifetime. It could be explained that the vapor density is much larger in higher system pressure and results in lower volumetric condensing rate.

Fig. 11 shows the comparison of bubble lifetime versus subcooled degree between different initial diameter and the 20 mm condensing bubble prediction of Sudhoff et al. (1982), which is a semi-empirical correlation based on the literature review since 1965, under the system pressure of 1 atm. The comparison is found in perfect agreement between the computational result and the correlation. The simulation and correlation indicate that as bubble initial diameter decreases, the lifetime versus subcooled degree line become closed. And the bubble lifetime has a rapidly decrease during the low subcooled degree region, but tends to be steady as the subcooled degree is large enough. Since the bubble lifetime is determined by subcooled degree, bubble initial diameter and fluid thermodynamic properties, once subcooled degree changes, the fluid thermodynamic properties changes as well, which thus leads to a non-linear relation between bubble lifetime and the subcooled degree.

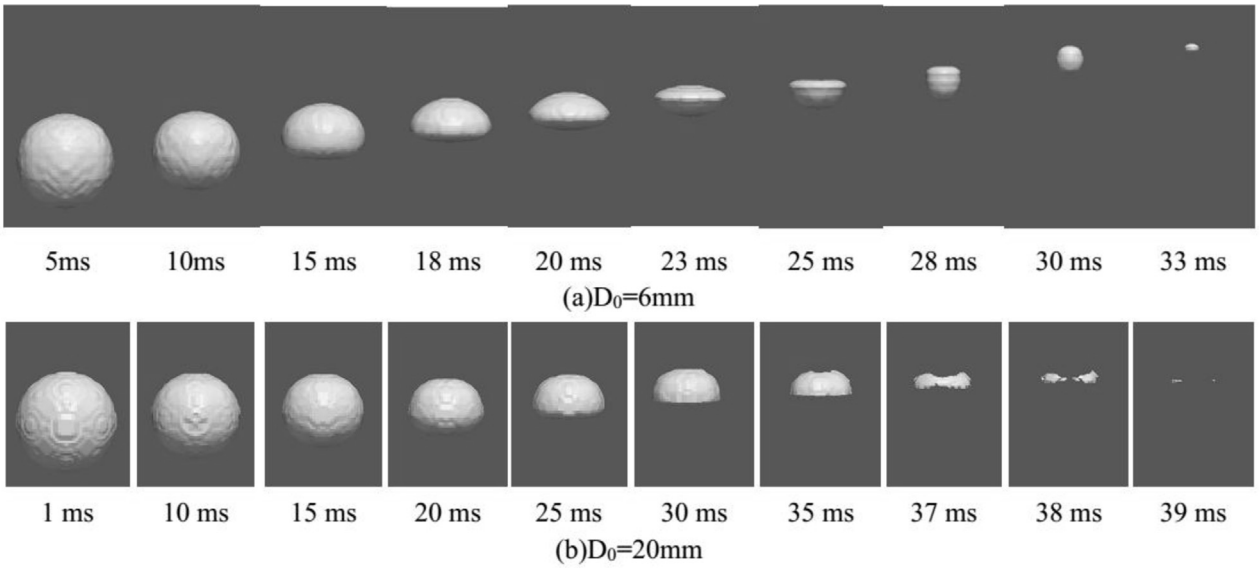

Fig. 7. Bubble shape sequences of different initial diameter during condensation (P = 1.55 MPa).

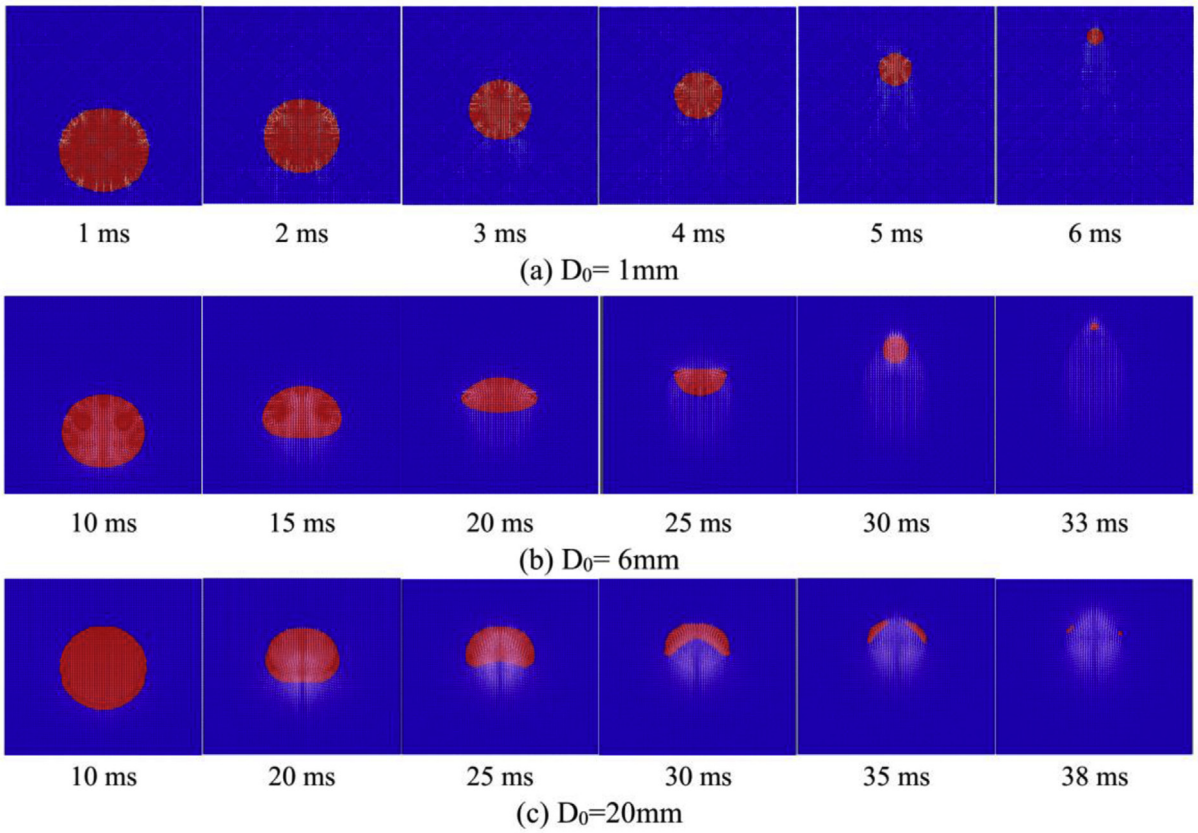

Fig. 8. Shape and flow field around bubbles with 1 mm, 6 mm and 20 mm initial diameter of three condensing processes (P = 0.1 MPa, ΔT_{sub} = 10 K).

3.5. Bubble diameter history and condensate Nusselt number

In many multiphase codes such as FLUENT and STAR, which solve the phase-averaged equations using Eulerian approach, the bubble condensation process must be effectively represented by a closure relation that describes the heat transfer from the vapor to the liquid phase in the energy equations, and a corresponding mass transfer term in the mass equations and a fraction transfer term in averaged phase fraction equation. Therefore, accurate prediction of the bubble size and condensing heat transfer is important to simulate subcooled flow successfully.

Many studies have been performed previously to develop correlations for bubble diameter history β and condensing Nusselt number Nu_c (Isenberg and Sideman, 1970; Chen and Mayinger,

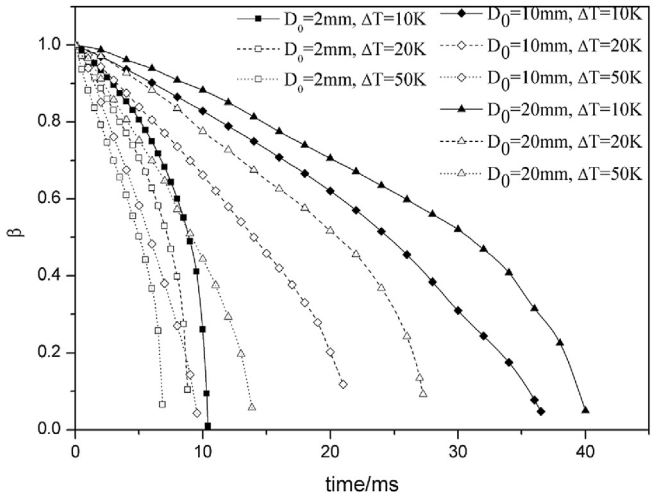

Fig. 9. Bubble diameter history.

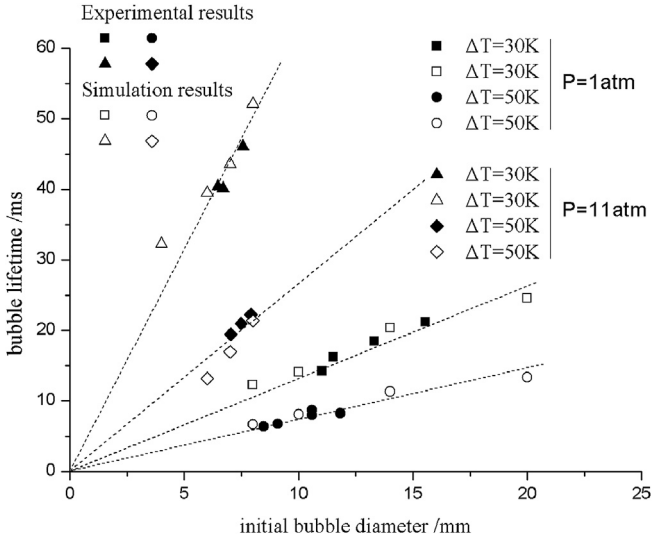

Fig. 10. Comparison on bubble lifetime in condensation between experimental and simulation results.

1992; Warrier et al., 2002). A listing of the most popular correlations and their applicability is given in Table 2. The condensate Nusselt number Jakob number, Fourier number, Bubble Reynolds number, and interfacial heat transfer coefficient are defined as follow:

$$\mathrm{Fo} = \frac{\alpha t}{D_0^2} \tag{17}$$

$$Re_b = \frac{\rho_l U_{rel} D_b}{\mu} \tag{18}$$

$$\mathrm{Ja} = \frac{\rho_l c_l (T_{sat} - T_l)}{\rho_v h_{lv}} \tag{19}$$

$$Nu_c = \frac{h_c D_b}{\lambda_l} \tag{20}$$

$$h_c = \frac{j h_{lv}}{A(T_{sat} - T_l)} \tag{21}$$

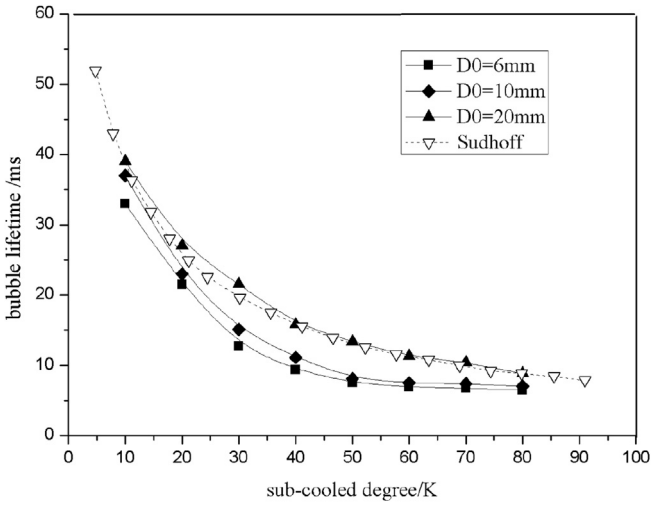

Fig. 11. Comparison of bubble lifetime between different initial diameter and Sudhoff's prediction.

where α is the thermal diffusivity of the liquid ($\alpha = \lambda_l/\rho_l c_l$), Re_{bo} is the bubble Reynolds number based on D_0.

In most study, β is a function of $Re_{b0,}$ Ja, Pr_l, and Fo number. Fig. 12 shows a comparison of the calculated β values in our cases and those predicted using correlations in Table 2, versus Fourier number under the same Re_{b0}, Ja, and Pr_l number. The square symbol, solid, dash and dash-dot lines indicate the bubble history of the simulation, Chen and Mayinger, Warrier et al., Isenberg and Sideman models, respectively. It can be seen that our numerical result is coincident with the prediction of Chen and Mayinger while underestimated with correlations of Warrier et al. and Isenberg and Sideman. That is because the bubble condensation in this study was investigated in subcooled region far from the heated wall, and differed from the previous studies (Warrier et al., 2002; Isenberg and Sideman, 1970) which were probably with the effect of heated wall. This also means that the bubble condensation in the heated region was longer than that in the unheated region. A comparison of more computational data and the corresponding predicted values (Chen and Mayinger, 1992) are shown in Fig. 13. From Fig. 13 it can be seen that the agreement between the simulation and the prediction of Chen and Mayinger is good. It is noted that, among those variables in the correlation expression, Ja plays a most important role in the bubble collapse (with order of 1, while others less than 1). Thus, with high Ja, which correspond to a much higher subcooling, the bubble size will decrease rapidly, and other effect could be neglect.

Condensate Nusselt number Nu_c is usually treat as a function of bubble Reynolds and Prandtl number in experimental correlations and averaged equations multiphase flow modeling. Fig. 14 shows a comparison of computational data and the prediction of Chen and Mayinger in Nu_c, the computational results match the predicted results greatly. It should be noted that although the dependence of Nu_c on time is not explicit, it is implicitly included in Re_b ($Re_b = \beta Re_{b0}$, where β is a function of time).

3.6. Drag coefficient

Assuming quasi-steady-state equilibrium of the drag, gravity, and buoyancy force for a bubble, the drag coefficient can be written as:

$$Cd = \frac{4}{3}\frac{D_b g(\rho_l - \rho_v)}{\rho_l U_b^2} \tag{22}$$

Table 2
List of dimensionless bubble diameter and condensation Nusselt number correlations.

Reference	Applicability	Bubble diameter	Nusselt number
Isenberg and Sideman (1970)	$3 < D_0 < 10$, mm	$\beta = (1 - 3/\pi^{1/2} JaRe_{b0} Pr_l^{1/3} Fo)^{2/3}$	$Nu_c = 1/\pi^{1/2} Re_b^{1/2} Pr_l^{1/3}$
Chen and Mayinger (1992)	$Re_b < 10{,}000$, $2 < Pr_l < 15$, $Ja < 80$	$\beta = (1 - 0.56 Re_{b0}^{0.7} Pr_l^{0.5} JaFo)^{0.9}$	$Nu_c = 0.185 Re_b^{0.7} Pr_l^{1/2}$
Warrier et al. (2002)	$20 < Re_b < 700$, $1.8 < Pr_l < 2.9$, $12 < Ja < 100$	$\beta^{3/2} = 1 - 1.8 Re_{b0}^{1/2} Pr_l^{1/3} JaFo_0 (1 - 0.72 Ja^{9/10} Fo^{2/3})$	$Nu_c = 0.6 Re_b^{1/2} Pr_l^{1/3} (1 - 1.20 Ja^{9/10} Fo^{2/3})$

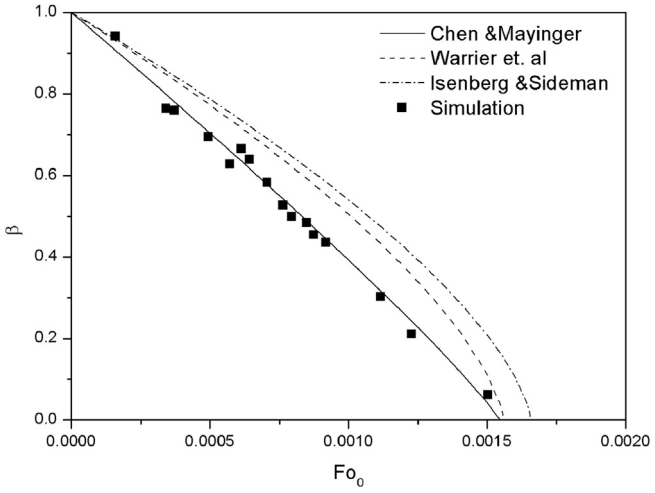

Fig. 12. Bubble history comparison between simulation and correlation ($Ja = 20$, $Re_{b0} = 200$).

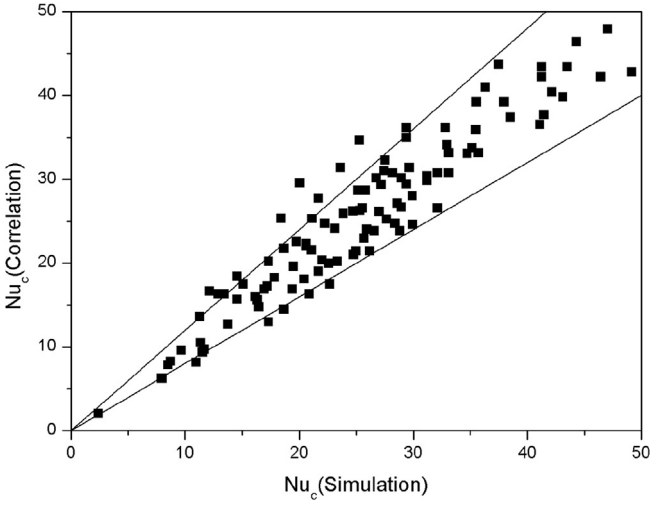

Fig. 14. Condensate Nusselt number comparison between simulation and correlation.

Based on our computational data, the corresponding bubble drag coefficient, *Cd*, which is obtained from Eq. (22), is plotted against bubble Reynolds number, on a log–log scale coordinate, as shown in Fig. 15. The standard drag coefficient for rigid spheres is calculated from Eq. (23) (Beard and Pruppacher, 1969) and is represented by a solid line in Fig. 15.

$$Cds = 24/Re \quad \text{for } \mathrm{Re} \le 1 \tag{23a}$$

$$Cds = 24/Re\left[1 + 0.102Re^{0.955}\right] \quad \text{for } 0.2 < \mathrm{Re} \le 1 \tag{23b}$$

$$Cds = 24/Re\left[1 + 0.115Re^{0.802}\right] \quad \text{for } 2 < \mathrm{Re} \le 21 \tag{23c}$$

$$Cds = 24/Re\left[1 + 0.189Re^{0.632}\right] \quad \text{for } 21 < \mathrm{Re} \le 200 \tag{23d}$$

$$Cds = 0.28 + 6/Re^{0.5} + 21/Re \quad \text{for } 200 < \mathrm{Re} \le 4000 \tag{23e}$$

The fluid-sphere model (Eq. (24)) from Hadamard (1911) is also used for predicting *Cd*, and is represented by a dash-dot line:

$$Cd = 16/Re \quad \text{for} \quad \mathrm{Re} < 1 \tag{24a}$$

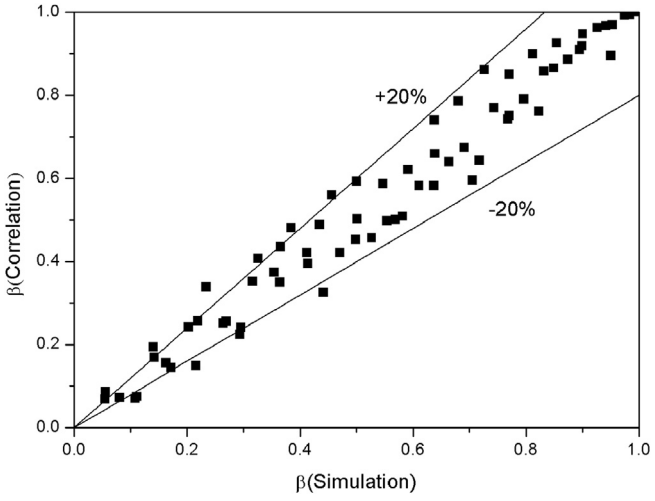

Fig. 13. Bubble history comparison between simulation and correlation.

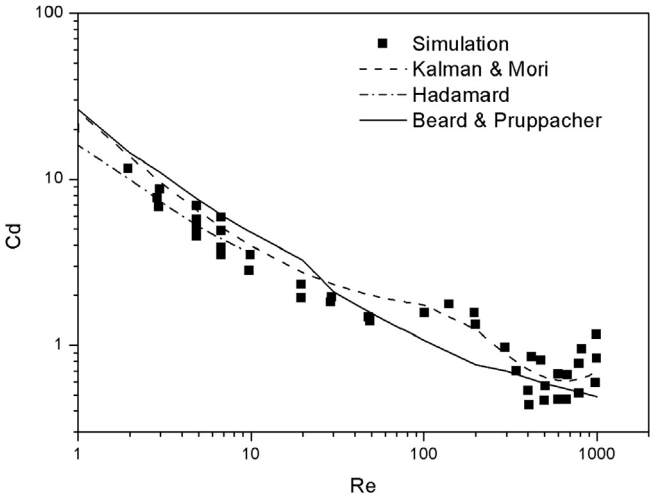

Fig. 15. Comparison of drag coefficient versus *Re*.

$$Cds = 16/Re[1 + Re/8] \quad \text{for } 1 < \mathrm{Re} \leq 10 \tag{24b}$$

Fig. 15 clearly indicates that the condensing bubble experiences a lower drag compared to that of a solid sphere of an equivalent size, up to a Reynolds number of 100, which is also observed in experimental result of Wanchoo et al. (1997). Kalman and Mori (2002) improved the correlation based on their relevant experimental results, their prediction is represented by dash line in Fig. 15, however the oscillation problem in high *Re* is still unsolved.

$$Cd = \frac{24}{Re} + \frac{1}{5 + Re} + 1.5 \quad for\ 0.05 < Re < 100 \tag{25a}$$

$$Cd = \frac{240}{Re} + 1.44 \times 10^{-5} Re^{1.5} \quad for \quad 100 < Re < 2000 \tag{25b}$$

Wanchoo et al. pointed out that the reduction in the drag coefficient of a condensing bubble is due to the presence of a mobile interface (condensate film) and a high degree of internal circulation present within the bubble. In order to achieve a correlation for *Cd*, they introduced a reduced drag coefficient which was defined as in Eq. (26) and a new dimensionless variable, *W*, standing for influence of bubble size reducing, defined as in Eq. (27).

$$Cdr = Cd/Cds \tag{26}$$

$$W = \left[D_b g^{2/3} \Delta\rho^{2/3}\right] \Big/ \left[u \mu_l^{1/3} \rho_l^{1/3}\right] \tag{27}$$

Fig. 16 shows a relation between *Cdr* and *W* of the computational data, comparing the proposed correlation of Wanchoo et al. It can be seen that simulation and empirical correlation are with good agreement and both of them indicate a reduced drag coefficient is appropriate and necessary in drag force modeling.

4. Conclusions

In this paper, the behavior of condensing bubble was numerically investigated by using OpenFOAM. The coupled of Volume of Fluid and Level Set method, which combines the advantages of both VOF and LS, was developed and implemented in the code. And the phase change model for condensation also developed and implemented in the code. The numerical model was validated by comparing the numerical results in this study with the experimental results. Furthermore, the behavior of condensing bubbles was investigated qualitatively under various conditions. The bubble deformation, bubble lifetime, bubble size history, condensate Nusselt number and other interesting parameters have been obtained and analyzed in detail.

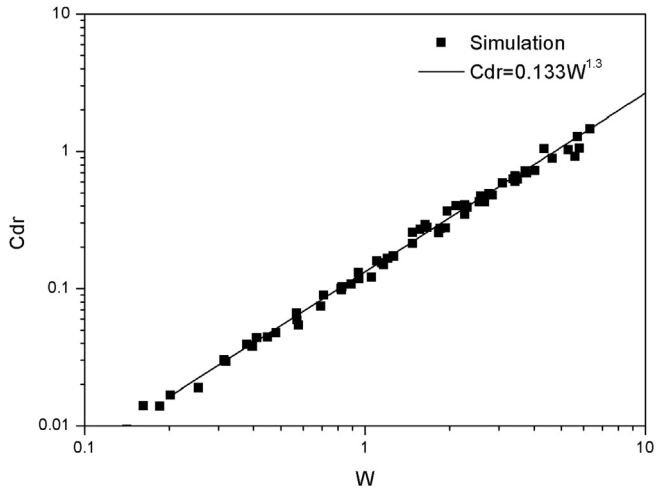

Fig. 16. Comparison of reduced drag coefficient.

(1) Bubble deformation is influenced greatly by initial diameter and degree of liquid subcooling. Bubble deformation will be more intense with increasing subcooling and initial diameter. A larger bubble experiences more severe deformation at lower degrees of liquid subcooling while the bubble deformed little at higher liquid subcooling degrees. Bubble will be pierced when the subcooling and initial diameter reach a certain value at the later condensing stage.
(2) The bubble diameter decreases when bubble size and subcooled degree is low. As a piercement happens in large bubble and high subcooling, bubble diameter will decrease rapidly. The bubble lifetime in condensation increases as bubble initial size increases, while with increasing subcooling, the bubble lifetime reduces significantly and will be prolonged at higher system pressure.
(3) The bubble diameter history and condensate Nusselt number in simulation are in good agreement with the correlation of Chen and Mayinger. The drag force coefficient was predicted well by introducing a reduced drag coefficient.

Acknowledgments

This work is partially supported by Open Research Fund Program of Key Laboratory of Advanced Reactor Engineering and Safety, Ministry of Education of China (Grant No. ARES-200401), and the Program for New CenturyExcellent Talents in University (Grant No. NCET-10-0846). Appreciation is also due to the OpenFOAM team for the contribution to the wonderful open-source CFD tool OpenFOAM.

References

Albadawi, A., Donoghue, D.B., Robinson, A.J., Murray, D.B., Delauré, Y.M.C., 2013. Influence of surface tension implementation in volume of fluid and coupled volume of fluid with level set methods for bubble growth and detachment. Int. J. Multiph. Flow. 53, 11–28.
Aufiero, M., Brovchenko, M., et al., 2014. Calculating the effective delayed neutron fraction in the molten salt fast reactor: analytical, deterministic and Monte Carlo approaches. Ann. Nucl. Energy 65, 78–90.
Beard, K., Pruppacher, H.R., 1969. A determination of the terminal velocity and drag of small water drops by means of a wind tunnel. J. Atmos. Sci. 26 (5), 1066–1072.
Brackbill, J.U., Kothe, C., Zemach, D.B., 1992. A continuum method for modeling surface tension. J. Comput. Phys. 100 (2), 335–354.
Cai, J.J., Watanabe, T., 2011. Numerical simulation of thermal stratification in cold legs by using OpenFOAM. Prog. Nucl. Sci. Tech. 2, 107–113.
Cai, J.J., Watanabe, T., Nakamura, H., 2010. Simulation of temperature stratification during ECCS water injection by OpenFOAM. In: 2010 Annual Meeting of the Atomic Energy Society of Japan, Mito, Ibaraki-ken, Japan, Mar. 26–28 (2010), [CD-ROM].
Cai, J.J., Zeng, Q.Y., Watanabe, T., 2013. OpenFOAM based numerical simulation on rising characteristics of bubbles. Therm. Power Gener. 42, 28–31.
Chen, Y.M., Mayinger, F., 1992. Measurement of heat transfer at the phase interface of condensing bubbles. Int. J. Multiph. Flow 18 (6), 877–890.
Chen, R.H., Tian, W.X., Su, G.H., Qiu, S.Z., Ishiwatari, Y., Oka, Y., 2010. Numerical investigation on bubble dynamics during flow boiling using moving particle semi-implicit method. Nucl. Eng. Des. 240, 3830–3840.
Chen, R.H., Tian, W.X., Su, G.H., Qiu, S.Z., Ishiwatari, Y., Oka, Y., 2011. Numerical investigation on coalescence of bubble pairs rising in a stagnant liquid. Chem. Eng. Sci. 66, 5055–5063.
Clift, R., Grace, J.R., Weber, M.E., 1978. Bubbles, Drops, and Particles. Courier Corporation.
Deshpande, S.S., Anumolu, L., Trujillo, M.F., 2012. Evaluating the performance of the two-phase flow solver interFoam. Comput. Sci. Discov. 5 (1), 014016.
Hadamard, J.S.C.R., 1911. Mouvement permanent lent d'une sphere liquide et visqueuse dans un liquide visqueux. CR Acad. Sci. 152 (25), 1735–1738.
Harada, T., Nagakura, H., Okawa, T., 2010. Dependence of bubble behavior in subcooled boiling on surface wettability. Nucl. Eng. Des. 240, 3949–3955.

Hardt, S., Wondra, F., 2008. Evaporation model for interfacial flows based on a continuum-field representation of the source terms. J. Comput. Phys. 227 (11), 5871–5895.
Isenberg, J., Sideman, S., 1970. Direct contact heat transfer with change of phase: bubble condensation in immiscible liquids. Int. J. Heat Mass Transf. 13 (6), 997–1011.
Jareteg, K., Vinai, P., Demazière, C., 2014. Fine-mesh deterministic modeling of PWR fuel assemblies: proof-of-principle of coupled neutronic/thermal–hydraulic calculations. Ann. Nucl. Energy 68, 247–256.
Ju, S.H., No, H.C., Mayinger, F., 2000. Measurement of heat transfer coefficients for direct contact condensation in core makeup tanks using holographic interferometer. Nucl. Eng. Des. 199, 75–83.
Kalman, H., 2003. Condensation of bubbles in miscible liquids. Int. J. Heat Mass Transf. 46 (18), 3451–3463.
Kalman, H., Mori, Y.H., 2002. Experimental analysis of a single vapour bubble condensing in subcooled liquid. Chem. Eng. J. 85, 197–206.
Kamei, S., Hirata, M., 1986. Condensation phenomena of single vapor bubble into subcooled water (1st report, flow visualization). JSME Ser. B 464–469.
Kamei, S., Hirata, M., 1990. Condensing phenomena of a single vapor bubble into subcooled water. Exp. Heat Transf. 3 (2), 173–182.
Kunkelmann, C., Stephan, P., 2009. CFD simulation of boiling flows using the volume-of-fluid method within OPENFOAM. Numer. Heat Transf. A Appl. 56 (8), 631–646.
Lin, M., Chen, P.P., 2012. Photographic study of bubble behavior in subcooled flow boiling using R-134a at low pressure range. Ann. Nucl. Energy 49, 23–32.
Morita, K., Matsumoto, T., Fukuda, K., Tobita, Y., Yamano, H., Sato, I., 2008. Experimental verification of the fast reactor safety analysis code SIMMER-III for transient bubble behavior with condensation. Nucl. Eng. Des. 238, 49–56.
Nath, D., Verma, M.K., 2014. Numerical simulation of convection of argon gas in fast breeder reactor. Ann. Nucl. Energy 63, 51–58.
OpenFOAM, 2014. OpenFOAM User's Guide, OpenCFD Limited.
Pan, L.M., Tan, Z.W., Chen, D.Q., Xue, L.C., 2012. Numerical investigation of vapor bubble condensation characteristics of subcooled flow boiling in vertical rectangular channel. Nucl. Eng. Des. 248, 126–136.
Patel, G., Tanskanen, V., Kyrki-Rajamäki, R., 2014. Numerical modelling of low-Reynolds number direct contact condensation in a suppression pool test facility. Ann. Nucl. Energy 71, 376–387.
Robin, T.T., Snyder, N.W., 1970. Theoretical analysis of bubble dynamics for an artificially produced vapor bubble in a turbulent stream. Int. J. Heat Mass Transf. 53, 11–28.
Rusche, H., 2002. Computational Fluid Dynamics of Dispersed Two-phase Flows at High Phase Fractions (Ph.D. thesis). University of London, UK.
Schrage, R.W., 1953. A Theoretical Study of Interphase Mass Transfer. Columbia University Press, New York.
Sudhoff, B., Plischke, M., Weinspach, P.M., 1982. Direct contact heat transfer with change of phase-condensation or evaporation of a drobble. Ger. Chem. Eng. 5, 24–43.
Sussman, M., Puckett, E.G., 2000. A coupled level set and volume-of-fluid method for computing 3d and axisymmetric incompressible two-phase flows. J. Comput. Phys. 162, 301–337.
Tian, W.X., Ishiwatari, Y., Ikejiri, S., Yamakawa, M., Oka, Y., 2010. Numerical computation of thermally controlled steam bubble condensation using moving particle semi-implicit (MPS) method. Ann. Nucl. Eng. 37 (1), 5–15.
Wanchoo, R.K., Sharma, S.K., Raina, G.K., 1997. Drag coefficient and velocity of rise of a single collasping two-phase bubble. AIChE J. 43 (8), 1955–1963.
Warrier, G.R., Basu, N., Dhir, V.K., 2002. Interfacial heat transfer during subcooled flow boiling. Int. J. Heat Mass Transf. 45 (19), 3947–3959.
Zeng, Q.Y., Cai, J.J., November 3~6, 2013. Numerical Simulation of Bubble condensation and Its Behaviour under Nonlinear Seismic Oscillation. The 13-th annual Meeting of Reactor Thermal Engineering and Fluid, Shanghai.
Zeng, Q.Y., Cai, J.J., 2014. Three-dimension simulation of bubble behavior under nonlinear oscillation. Ann. Nucl. Eng. 63, 680–690.
Zeng, Q.Y., Cai, J.J., Wantanabe, T., 2013. Simulation of oscillating free interface behavior by using OpenFoam. In: Proceedings of 21th International Conference on Nuclear Engineering (ICONE 21), Chengdu, 2013.
Zuo, J.L., Tian, W.X., Chen, R.H., Su, G.H., Qiu, S.Z., 2013. Two-dimensional numerical simulation of single bubble rising behavior in liquid metal using moving particle semi-implicit method. Prog. Nucl. Eng. 64, 31–40.